Influence of Hydrocortisone on the Mechanical Properties of the Cerebral Endothelium In Vitro

Sebastian Schrot,* Christian Weidenfeller,* Tilman E. Schäffer,[†‡] Horst Robenek,[§] and Hans-Joachim Galla*[‡]
*Institute for Biochemistry, and [†]Institute of Physics, Westfälische Wilhelms-Universität Münster Wilhelm-Klemm-Straße 2, 48149 Münster, Germany; [‡]Center for NanoTechnology, 48149 Münster, Germany; and [§]LIFA-Leibniz-Institute for Arteriosclerosis Research at the University of Münster, 48149 Münster, Germany

ABSTRACT Cerebral endothelial cells accomplish the barrier functions between blood and brain interstitium. Structural features are the tight junctions between adjacent endothelial cells and the formation of marginal folds at the cell-cell contacts. The glucocorticoid hydrocortisone (HC) has been reported to enforce the blood-brain-barrier in vitro measurable by an increase of the transendothelial electrical resistance. This study shows the impact of HC on the mechanical and morphological properties of confluent cell layers of brain microvascular endothelial cells. HC induces an increase in height of these marginal folds and a reduction of the intercellular contact surface. These morphological changes are accompanied by changes in cell elasticity. Staining of fibrous actin indicates that HC induces a reorganization of the actin cortex. The quantitative determination of the local elastic properties of cells reveals for the first time an HC-induced increase of the representative Young's modulus according to cytoskeletal rearrangements. For this study, cells of two different species, porcine brain capillary endothelial cells and murine brain capillary endothelial cells, were used yielding similar results, which clearly demonstrates that the HC effect on the cell elasticity is species independent.

INTRODUCTION

The blood-brain-barrier (BBB) regulates the transfer of compounds between the circulating blood stream and the interstitial fluid. Thus, the barrier ensures a constant internal environment in brains of vertebrates to sustain cerebral functions, especially neuronal activity, independently of concentration fluctuations of blood components. Brain capillaries are lined with a single endothelial cell layer at their luminal surface (brain capillary endothelial cells (BCEC)). The main characteristic structural feature of BCEC is the formation of continuous tight junctions at the intercellular cleft between adjacent cells (1–3). Tight junctions are the prominent structure of this nonfenestrated endothelium preventing the diffusive permeation of blood-derived hydrophilic substances. However, tight junctions are not the only molecular structures that contribute to the barrier properties. Despite this diffusive intercellular barrier, lipophilic solutes are able to permeate the BBB due to their membrane solubility (4,5). Thus, as a second feature, the endothelium is provided with a variety of specific active drug transport systems extruding invaded substances of the cells back into the bloodstream (6).

In vitro models of the blood-brain-barrier are often used to mimic the in vivo situation. Hoheisel et al. established a well-characterized serum-free porcine model of the BBB in vitro. Transendothelial electrical resistance measurements and drug transport investigations across the BBB under various experimental conditions have proven the existence of the in vitro barrier function, even in the absence of neighboring astrocytes (7).

Apically arranged tight junctions are the outstanding structural elements of intercellular contacts in epithelial and cerebral endothelial cells (8). In comparison to endothelial cells of peripheral capillary vessels, tight junctions of the cerebral endothelium are generally more extensively structured (9). A structural feature along the contact zone of neighbored endothelial cells is an elevated cell-overlapping area. These areas are known in vivo as marginal folds and are also observable in cell culture (9).

The incubation of porcine BCEC with the glucocorticoid hydrocortisone (HC) induces an increase in transendothelial electrical resistance and therefore an increase of the barrier function of the BBB in vitro (7). At a concentration of 550 nM HC in the medium, the maximum effect could be observed (7). The increase of the transendothelial electrical resistance is accompanied by the accretion of marginal folds at the cell-cell contacts (10). Here, the scanning force microscopy (SFM) has been used to measure the height of such cellular protrusions in cell cultures as a marker for a well-developed barrier. The question of whether these morphological changes go along with cytoskeletal rearrangements is addressed in this study by the SFM technique on living cells. Two mammalian in vitro models with characteristic BBB features such as high transendothelial resistance and well-developed tight junctions under the same conditions are available for biophysical characterization.

In basic experiments, Henderson et al. observed the dynamic behavior of the cytoskeleton of living glial cells by SFM (11). Tao and colleges used SFM for the first time for a quantitative determination of elastic properties of biological material (12).

Submitted December 30, 2004, and accepted for publication August 26, 2005.

Address reprint requests to Hans-Joachim Galla, E-mail: gallah@uni-muenster.de.

0006-3495/05/12/3904/07 $2.00

doi: 10.1529/biophysj.104.058750

Locally resolved and quantitative maps of sample elasticity can be acquired by repeated recording of force curves while the tip scans laterally across the sample (''force mapping mode'') (13–16). From this set of force curves the sample topography as well as the local elastic modulus can be calculated according to the Hertzian model for elastic indentations (17,18). The force mapping technique combines the imaging of viscoelastic properties and the visualization of cell topography. It is sometimes gentler than other imaging modes (e.g., contact mode, tapping mode) due to the absence of lateral forces and friction during the measurement (19).

In earlier studies, the enforcement of the barrier has been followed in living cells by impedance spectroscopy (7). However, this technique only allows one to measure the electrical conductivity established by the tight junctions but also the interaction of the endothelial cell with their extracellular matrix. Using immunofluorescence techniques yields information about the cytoskeletal reorganization, however, for this technique, cells have to be chemically fixed. Here, we have applied SFM to measure the elasticity of living murine and porcine cells reflecting the cytoskeletal arrangement under the influence of the barrier enhancing glucocorticoid HC. In addition, the formation of the marginal folds has been quantified by its height.

MATERIALS AND METHODS

Preparation of PBCEC

Porcine brain capillary endothelial cells (PBCEC) were isolated from freshly slaughtered pigs as described previously (20) and seeded in culture flasks coated with Collagen-G. Cells were cultured at 37°C in humidified air and 5% CO2 in Eagle's Medium 199 containing 0.7 mM L-glutamine (both Biochrome KG, Berlin, Germany), 10% fetal calf serum (Gibco Life Technologies, Eggenstein, Germany), 100 μg/ml penicillin/streptomycin, and 100 μg/ml gentamycin (both Biochrome KG). The primary cultured PBCEC were trypsinated after 48 h and seeded on Collagen-G (Biochrome KG) coated LABTEK chamber slides (Nalge Nunc International, Naperville, IL). After the cell reached confluence, in vitro medium was replaced by DMEM/Ham's F 12 (Biochrome KG) containing 0.7 mM L-glutamine, 100 μg/ml penicillin/streptomycin, 100 μg/ml gentamycin (all Biochrome KG), and if required 550 nM HC (Sigma-Aldrich GmbH, Steinheim, Germany) but no serum. Measurements on PBCEC were performed after 7 days in vitro.

Preparation of murine brain capillary endothelial cells

Isolation of murine brain capillary endothelial cells (MBCEC) from 6- to 10-week-old mice (C57BL6/J) followed a modified protocol of Deli et al. (21). MBCEC were seeded on collagenIV/fibronectin-coated petri dishes (Sigma-Aldrich GmbH) in culture medium, DMEM (Biochrome KG) containing 20 vol % plasma-derived serum (FirstLink, Birmingham, UK), 1 ng/ml basic fibroblast growth factor (Boehringer Mannheim, Germany), 1 μg/ml heparin (Sigma-Aldrich GmbH), 100 μg/ml gentamycin, and 0.7 mM L-glutamine (both Biochrome KG) and 4 μg/ml puromycin (Alexis GmbH, Grünberg, Germany). After 24 h, medium was renewed, again supplemented with 4 μg/ml puromycin; 48 h after plating, this medium was replaced with puromycin-free culture medium.

Within 3 days, cells usually reach 80% of confluence. The primary cultured MBCEC were trypsinated and subcultured in culture medium (replenished DMEM) on Collagen-G (Biochrome KG) coated LABTEK chamber slides (Nalge Nunc International). After 48 h, medium was replaced by serum-free medium supplemented by 550 nM HC (Sigma-Aldrich GmbH), if required. Measurements were performed after 7 days in culture.

Transmission electron microscopy

After reaching 70–80% of confluence, MBCEC were subcultured on rat tail collagen-coated microporous polycarbonate filter membranes (Transwell, Costar GmbH, Bodenheim, Germany). After reaching confluence, cells were washed twice with PBS and fixed for 1 h in sodium cacodylate buffer (0.1 M sodium cacodylate, 2.5% glutaraldehyde, 2 mM $CaCl_2$) at room temperature. Samples were washed with water (30 min, shaker) and incubated for 45 min at room temperature in 0.5% (w/v) OsO_4 solution in sodium cacodylate buffer followed by a second washing step for 30 min in water. Subsequently, the samples were dehydrated by incubation in 75% (v/v) ethanol, then 100% ethanol, and finally propylene oxide for 5 min. After incubation in a mixture of propylene/epon (1:1) for 30 min the samples were incubated in pure epon for 15 min. Finally, the samples were embedded in pure epon containing mold and dried for 24–48 h at 60°C. Ultrathin sections were examined and photographed using a Philips EM 201 (Eindhoven, The Netherlands).

Scanning force microscopy

Imaging and elasticity measurements were performed using a commercial SFM (Bioscope, Digital Instruments, Santa Barbara, CA). Before experiments, the medium was replaced by PBS and tempered at 37°C (heated from below by a homebuilt, Peltier heated brass chamber, PID-controlled). Soft cantilevers were used with a spring constant of <0.01 N/m (Microlever, Park Scientific, Santa Clara, CA) as determined by the thermal noise method (22). Surface images were performed by using contact mode, tip velocity 100–200 μm/s, 512 $\times$ 512 dots per image.

To obtain the images of the local Young's modulus, the SFM was operated in force mapping mode, which gathered a two-dimensional array of 64 $\times$ 64 force-distance curves while scanning across the sample surface. Force-distance curves were acquired at a rate of 2.5 Hz. One complete force map was recorded in 90 min. To minimize mechanical strain of the underlying biological sample and to ensure an exclusive indentation of the top of the cell layer only, the maximum applied force was limited to 350–500 pN. The calculation of local Young's modulus was done by using the Hertzian model of elastic indentations with Sneddon's modifications (14,18).

Data are presented as mean values $\pm$ SE. Number of measurements (n) is 16 in case of the height determination of the marginal folds and $n = 12$ for the determination of the Young's modulus.

Fluorescence microscopy

Cells were fixed with 4% (w/v) paraformaldehyde (Merck KG, Darmstadt, Germany) in PBS solution for 15 min., rinsed with PBS, permeabilized for 10 min with 0.2% Triton-X 100 (Serva Feinbiochemica GmbH, Heidelberg, Germany) in PBS solution supplemented with 3% (v/v) normal goat serum (Sigma-Aldrich GmbH) to block nonspecific binding sites, and rinsed with PBS.

For actin staining, cells were incubated with 0.3 μg/ml rhodamin-labeled phalloidin (Sigma-Aldrich GmbH; absorption maximum, 540–545 nm; emission maximum, 570 nm in ethanol) in PBS for 45 min and then rinsed with PBS. Fluorescence images were acquired at an inverted optical microscope (fluorescence microscope DM IRB, Leica Microsystems AG, Wetzlar, Germany) using cut-off filter at 540–565 nm.

RESULTS

This study applies a well-established in vitro model for the blood-brain-barrier based on primary cultured PBCEC (7) and on MBCEC, both under serum-free conditions. Here, the

mechanical properties and the morphology of cells of both species were investigated after incubation of the cells with the glucocorticoid HC.

Morphological changes

After incubation of HC (550 nM), marginal folds emerge at cell junctions. The transmission electron microscopy (TEM) provides an established method to image ultrathin cross sections of the endothelial cell layer. The TEM images visualize even subcellular details of the specimen. TEM images reveal the typical profile shape of a HC-induced marginal fold. Fig. 1 shows TEM images of two adjacent MBCEC of a confluent cell layer. The formation of marginal folds cannot be observed at cells cultured in HC-free medium (Fig. 1 *A*). Marginal folds cover the junctional cleft between two adjacent cells. MBCEC cultured under serum- and HC-free conditions present a smooth apical cell surface and a largely extended cell-cell-contact zone (Fig. 1 *A*, *arrow*). The scheme of Fig. 1 *B* illustrates the appearance of the cell-cell-contact zone of HC-free cultured adjacent endothelial cells (*arrow*). Whereas HC-incubated MBCEC layers indicate the formation of marginal folds at the cell-cell-contacts (Fig. 1 *C*). The incubation of HC entails the formation of cell material that overlaps onto the apical membrane of the neighbored cell (Fig. 1 *C*, *arrow*). The intercellular contact zone (Fig. 1 *B*, *arrow*) is clearly reduced as Fig. 1 *D* schematically points up (*arrow*, *red line*). TEM profile images confirm the HC-depending accretion of marginal folds and reveal a decrease in overlapping zones (Fig. 1). The accretion of marginal folds is accompanied by a reduction of the intercellular contact surface.

Imaging cell topography by scanning force microscopy enables the investigation of ultrastructural changes of marginal fold profiles at cell junctional regions in living cells. Serum-free cultured adjacent PBCEC typically exhibit a spindle-like shape and weakly developed marginal folds at their cell-cell contacts (Fig. 2 *A*). The arrow in Fig. 2 *A* points to distinct actin fibers visible underneath the cell membrane. The image of Fig. 2 *A* illustrates the distribution of the fibers in the actin cortex. Fig. 2 *B* demonstrates the appearance of an HC-incubated PBCEC monolayer. The cell-cell contacts are clearly visible in the SFM image and the HC-treated PBCEC show perspicuously enlarged marginal folds (Fig. 2 *B*, *arrow*). Untreated MBCEC differ in morphology from PBCEC by featuring a cobblestone-shaped pattern (Fig. 2 *C*). The SFM images imply a HC-induced accretion of *marginal folds*. After HC incubation, the originally cobblestone-shaped MBCEC have adapted a spindle-like morphology (Fig. 2 *D*). The adaptation of the MBCEC to the HC-supplemented medium usually appears after a lapse of 8–10 h. Some MBCEC exhibit both shapes within the cell layer by forming domains of spindle-like shaped morphology in a carpet of cobblestone-shaped cells.

The TEM images of Fig. 1 already demonstrate the overlap of cell material at the cell-cell contacts after the incubation with HC. Differences in height of these protrusions at the cell-cell contacts were visualized by SFM height images and represent the accretion of marginal folds after of HC treatment.

Fig. 3 *A* shows a height image of a confluent MBCEC layer incubated with HC. The arrow points at the marginal folds that are accreted in response to the incubation with HC. The image of Fig. 3 *B* indicates a scan of the enlarged section (*red dashed-line square*) of Fig. 3 *A*. The image shows the detailed topography of a marginal fold of a living endothelial cell. The gap between the adjacent cells and the overlapping cell material is clearly recognizable (*arrow*). In this case, the shown gap exhibits a width of ~150–200 nm (Fig. 3 *B*).

Profile analyses provide the appropriate method for the quantitative determination of the height of the marginal folds. Fig. 4 shows the profile of the cell layer along the red dashed line of the image in Fig. 3 *B*. The height of the peaks in the profile image directly corresponds to the height of the marginal fold and allows the determination of the accretion of the marginal folds. The investigation of many of these

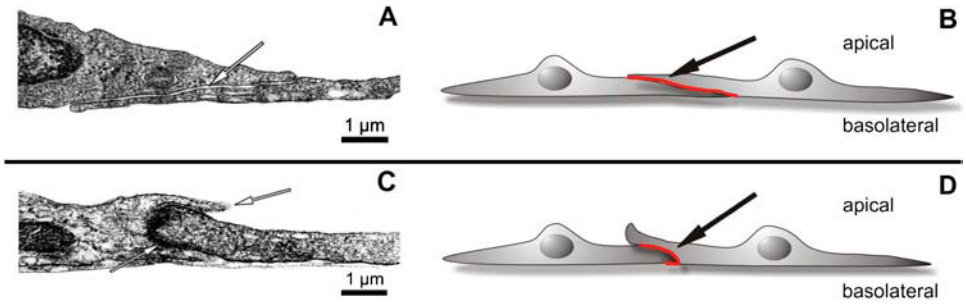

FIGURE 1 Transmission electron microscopy images of cultivated MBCEC on Transwell filter plates. Images show the profile of the cell layer of two adjacent cells. (*A*) Cell-cell contact zone of confluent MBCEC cultivated under serum-free conditions. MBCEC show no marginal folds and the cell-cell contact zone is typically developed (*arrow*). (*B*) Additional scheme of adjacent cells within an endothelial cell layer. Endothelial cells cultivated under serum-free conditions exhibit large contact zones at the intercellular cleft that illustrates the red line in the scheme (*arrow*). No marginal folds developed. (*C*) MBCEC cultivated in 550 nM HC supplemented medium. Characteristic formation of HC-induced marginal folds at the apically exposed cell surface (*top arrow*) and reduction of the cell-cell contact zone (*bottom arrow*). The increase of the transendothelial resistance entails a closer membrane contact. Hence, the contact zone of HC-incubated cells appears more electron dense than that of nontreated cells. (*D*) Scheme of adjacent cells within an endothelial cell layer. Endothelial cells cultured in HC-supplemented culture medium, apical formation of marginal folds and reduced cell-cell contact zones (*arrow*; *red line*).

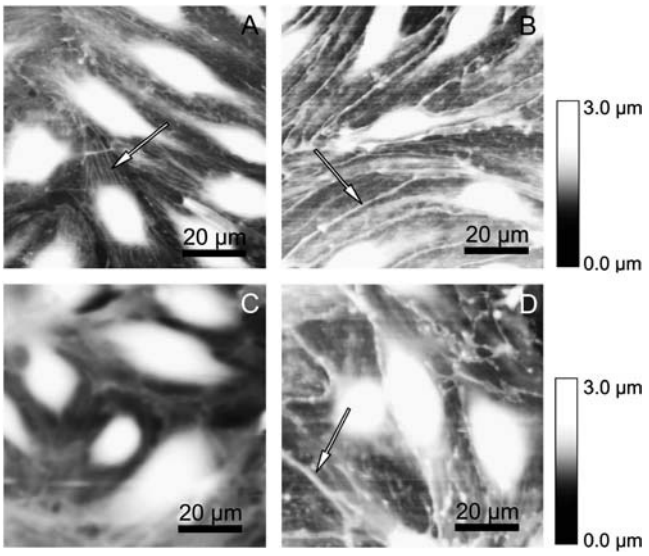

FIGURE 2 Scanning force microscopy. Height images of confluent endothelial cell layer. (*A*) PBCEC cultured under serum-free conditions. Cells appear in typical spindle-like shape. Actin fibers clearly emerge from the cytosol (*arrow*). (*B*) PBCEC cultured in HC-supplemented cell medium. Accretion of cell-cell contacts evidently developed (*arrow*). (*C*) Serum-free cultured untreated MBCEC. Cells appear in cobblestone-like shape. (*D*) MBCEC cultured in HC-supplemented medium. Cells clearly form marginal folds at the cell edges (*arrow*). MBCEC adapt spindle-like shapes.

profiles enables the quantitative determination of the accretion of marginal folds in response to the incubation with HC.

Profile analysis reveals that marginal folds of untreated PBCEC show an average altitude of 68 ± 12 nm ($n = 16$) (Fig. 5). The altitude of marginal folds of untreated MBCEC is 98 ± 13 nm ($n = 16$).

The HC-induced structural rearrangement occurs by an altitudinal increase of marginal folds. The marginal folds of HC-incubated PBCEC exhibit an altitude of 190 ± 42 nm ($n = 16$) and of HC-incubated MBCEC an altitude of 230 ± 42 nm ($n = 16$). After HC incubation, marginal folds accrete by a factor of 2.8 at PBCEC and by a factor of 2.4 in the case of MBCEC (Fig. 5).

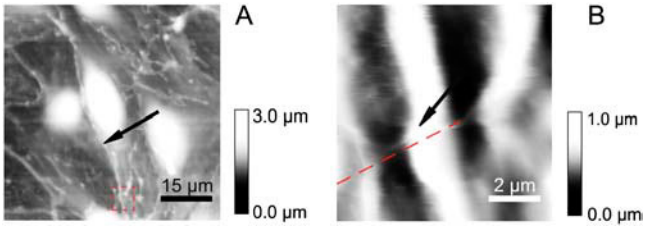

FIGURE 3 SFM images of MBCEC under physiological conditions. (*A*) Height image of a confluent cell layer cultivated in HC-containing medium. MBCEC developed marginal folds at the cell edges (*arrow*). (*B*) Hardware zoom in the square of image *A* (*square*). The image shows a detailed structure of the cell surface at the edges. Cell-cell contacts are overlapped by marginal folds (*arrow*).

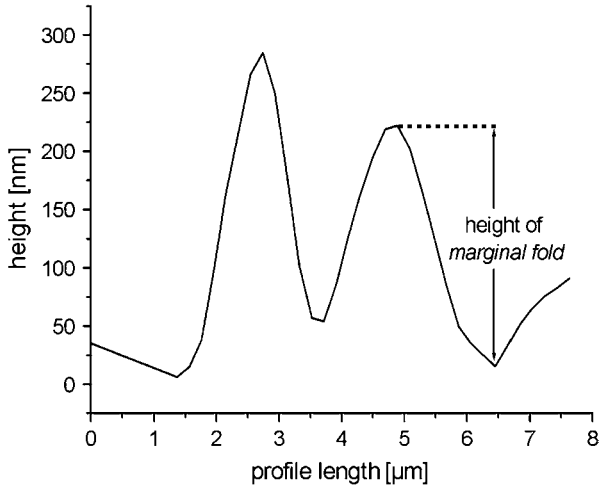

FIGURE 4 Height profile of an MBCEC layer of Fig. 3 *B* (*dashed line*). The altitude is determined by measuring the accretion of single profile peaks representing a marginal fold.

Elasticity changes

The force maps provided the base to calculate zero-force height images. Each zero-force height image (Fig. 6 *A*) was background-removed by subtracting a plane fit. A binary mask (Fig. 6 *B*) was produced from the background-removed zero-force height image by thresholding the image at 500-nm height. This excluded thin regions of the cells where the extracted Young's modulus might contain artifacts due to the presence of the underlying support surface. The mask was applied to the Young's modulus image (Fig. 6 *C*), and a representative Young's modulus was calculated as the median of the pixel values within the mask (areas higher than 500-nm height). The representative Young's modulus was therefore derived from the high regions that approximately correspond to the nuclear regions.

The formation of marginal folds seems to be part of an intracellular reorganization. Cell elasticity measurements provide an excellent technique for studying structural rearrangements. Force mapping experiments of HC-treated and untreated living cell samples reveal differences in the representative Young's modulus. Untreated PBCEC exhibit a representative Young's modulus of 5100 ± 1900 Pa

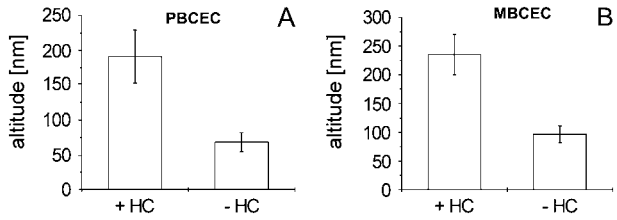

FIGURE 5 Results of marginal fold accretion study of PBCEC and MBCEC. (*A*) Confluent PBCEC layers indicate an obvious increase of marginal folds after HC incubation. (*B*) On confluent MBCEC supplementation of HC supports the development of marginal folds.

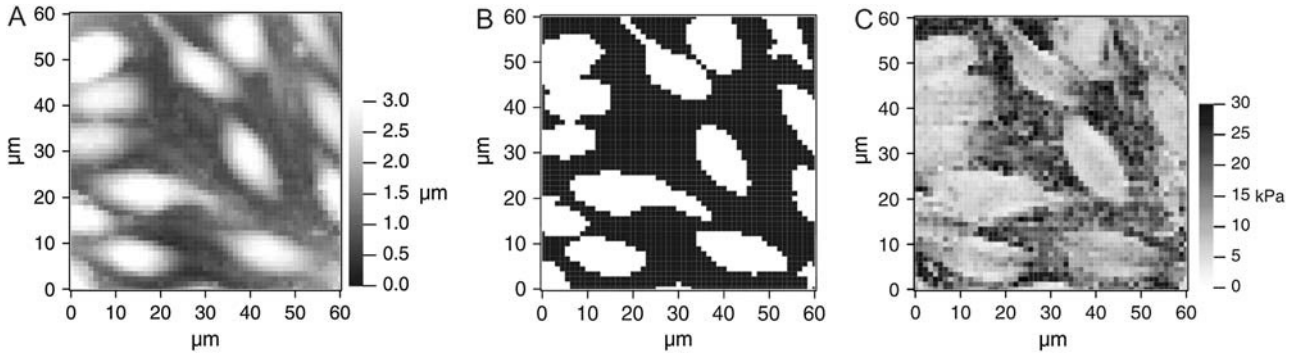

FIGURE 6 Force mapping mode images of serum-free cultured confluent PBCEC. (*A*) Zero-force height image. (*B*) Binary mask of the zero-force height image. The height threshold was 500 nm. Only data of white areas contribute to the determination of the representative Young's modulus; black areas were discarded. (*C*) Elasticity image, representing the two-dimensional distribution of the local Young's modulus on the sample surface.

($n = 12$). After incubation of HC, the representative Young's modulus of PBCEC rises up to 8300 ± 2600 Pa ($n = 12$). Similar results have been obtained by elasticity measurements of MBCEC. Serum-free cultured MBCEC show a representative Young's modulus of 5000 ± 1400 Pa ($n = 12$). HC treatment increases the representative Young's modulus of MBCEC to 8700 ± 2400 Pa ($n = 12$) (Fig. 7). These results reveal a HC-induced increase of the representative Young's modulus of BCEC of both species by a factor of ~1.7 (*t*-test values: t(PBCEC) = 0.9873; t(MBCEC) = 0.9412).

Cytoskeletal rearrangements

Fibrous actin is one of the major compounds of the cytoskeleton. Its contractile properties and its linkage to the tight junctions moves fibrous actin into the focus of interest (23). HC may influence the redistribution of actin filaments and may induce previously described morphological changes. Untreated PBCEC exhibit the typical perijunctional ring, cell nuclei appear only lowly covered with actin strands (Fig. 8 *A*). Most of the actin fibers are longitudinally located along the cell margins.

After HC incubation fibrous actin is entirely spread over the interior of the cell. Distinct actin strands occur in longitudinal direction in the cytoplasm along the cell spindle cross-linked by smooth actin fibers (Fig. 8 *B*). On the apical cell side actin fibers overstretch the whole cell corpus. These fluorescence images clearly indicate HC-induced cytoskeletal rearrangements.

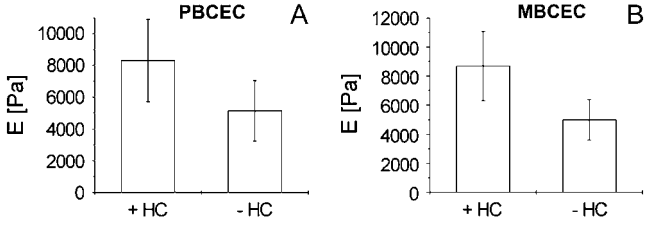

FIGURE 7 Results of the HC-induced elasticity changes at confluent PBCEC and MBCEC. (*A*) The incubation with HC induces a clear increase of the Young's modulus of PBCEC. (*B*) Similarly to panel *A*, the cell stiffness of MBCEC rises in response to the incubation with HC.

DISCUSSION

Tight junctions, adherens junctions, and the cytoskeleton represent an integrated functional unit of multiprotein complexes that seal the contact between adjacent barrier-forming cells (23–26). Elasticity investigations by SFM enable the characterization of cytoskeletal structures in living cells appearing in fixed cells used for immunofluorescence images (27).

Our results indicate that the reorganization of the actin cortex in response to HC contributes to the changes in the elastic properties of the cells. Under physiological conditions actin fibers and intermediary filaments influence the elastic properties of cells (27,28). Glucocorticoids are known to induce various cellular responses (29); e.g., the glucocorticoid dexamethasone (100 nM) and HC (100 nM) stabilize filamentous actin by an increased expression of actin-binding protein caldesmon in several cell types after 15-h incubation (30). The stabilization of actin increases the total amount of

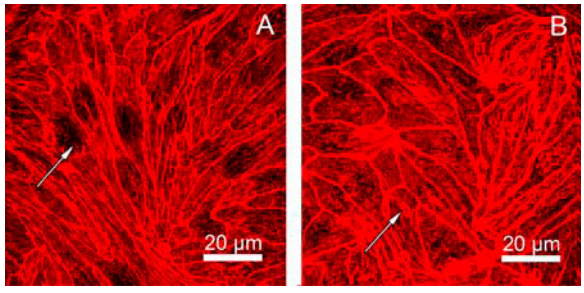

FIGURE 8 Fluorescence light microscopy images of rhodamin-phalloidin stained fibrous actin of PBCEC. (*A*) Untreated PBCEC indicate the distribution of fibrous actin under serum-free conditions in particular the perijunctional actin ring (*arrow*). (*B*) Distinct longitudinally orientated actin fibers signify HC-induced structural alteration (*arrow*). The accumulation of actin at the perijunctional ring appears enhanced.

cortical actin in the cytoplasm and subsequently results in higher cell stiffness. Additionally the glucocorticoid dexamethasone results in a reinforcement of actin bundles in NRK cells (30). Possibly the glucocorticoid-induced cytoskeletal reinforcement only occurs in cells with barrier functionality in vivo. Accordingly in terms of the cytostructural modifiablility of endothelial cells, the efficiency of HC still remains considerable. This study reveals an HC-induced increase of cell stiffness. Immunofluorescence images demonstrate perspicuous redistributions of fibrous actin within the cytoplasm.

Microtubules perform the organization of intermediate filaments within the cytoplasm (31). Application of agents disassembling single tubulin molecules (32) or drugs that stabilize microtubules by inducing tubulin polymerization (33), interrupts the distribution of cortical actin filaments. These drugs affecting the integrity of microtubule structures cause no degradation of cell elasticity (34). In addition, the application of the glucocorticoid dexamethasone (100 nM) had no effect on microtubules of different cell types (30). Presumably, microtubules might not contribute to the observed elasticity changes of PBCEC and MBCEC after HC incubation.

The mechanism of positioning cortical actin filaments has not been resolved yet (35). Microtubules are concentrated in the perinuclear region and do not support the apical membrane (36). Additionally, microtubules indicate no discernible impact on elasticity (37). The elasticity of living cells depends only on the distribution of the subapical actin network and consequently HC-induced elasticity changes originate from cytoskeletal rearrangements.

Using SFM, the applied pressure molds the cell membrane into the cytosol unless underlying structures reinforce membrane integrity. Images at zero loading force reveal the original appearance of the cell surface exhibiting no fibrous pattern. Actin filaments underlie dynamic structures related to the balance of polymerization and depolymerization at the filament ends as well as to the number of ends available for such exchange. The abundance of frequently exposed ends determines pivotally the dynamic and the turnover of the actin cortex. Glucocorticoids probably stabilize filamentous actin by reducing the formation of filament ends in correlation to the reinforcement of actin bundles (30). In accordance, this study reveals that the glucocorticoid HC leads to an increase of cell stiffness. Actin depolymerization agent cytochalasin D inhibits the cells own polymerization mechanism of filamentous actin. Incubation of cells with cytochalasin D reduces stiffness of cells and eliminates differences in stiffness. Obviously, cell stiffness originates from the subapical actin network (38).

The biological functionality of HC on the cytoskeleton has not been clearly elucidated yet (23). Confluent PBCEC and MBCEC layers show an HC-induced improve of the transendothelial electrical resistance (39), which depends on paracellular permeability. Tight junction proteins claudin and occludin are transmembrane components involved in formation of the paracellular barrier of cell layers (23). The cytoplasmic protein ZO-1 mediates a link to the perijunctional actin cytoskeleton and the tight junction proteins. Binding to ZO-1 is responsible for the functional positioning of occludin and for the transduction of regulatory signals on tight junctions and the actin cortex. Finally, the HC-induced cytoskeletal reconstruction and the occurring elasticity changes are accompanied by modifications of tight junctional integrity. Moreover, actin fiber staining confirms the dependency of these mechanical and morphological properties from the subapical actin network.

The enhancement of the marginal folds height of confluent cells after HC treatment and the increase of cell stiffness parallels the HC-induced improvement of the barrier function (39). Applying loading forces of 350–500 pN during imaging in contact mode enables destruction-free imaging of the cell surface and reproduces faithfully the ''real'' sample topography. Sensitive surface structures such as marginal folds occur under slight deformation during probe contact period. Concerning the determination of the accretion of marginal folds, indentations of the material of marginal folds are negligible due to the slightly applied loading forces. In comparison to living cells, additional analysis of fixed cell layers of untreated and HC-incubated PBCEC result in similar altitudes of marginal folds for each condition.

CONCLUSION

It is known that the glucocorticoid HC significantly improves the barrier properties of cerebral endothelial cells. The enhancement of the barrier is not accompanied by an upregulation of tight junction proteins. Cytoskeletal rearrangements occur and rearrangements of tight junction proteins like occludin and ZO-1 have been observed by immunofluorescence, which means fixed cells. Because cytoskeletal rearrangements of fibrous actin within the cytoplasm is expected to influence cell elasticity, we investigated cell elasticity by SFM. The increase of the representative Young's modulus after HC incubation clearly indicates that the observed intercellular rearrangements of cytoskeletal and probably also of the tight junction proteins occur in living cells excluding artifacts of the fixing process. Moreover, it was shown by the SFM height measurements, that the marginal folds that are always present at the BBB in vivo, develop under the influence of HC in cell cultures. This indicates that our cell cultures even in the absence of astrocytes in coculture develop barrier properties that are close to the in vivo situation.

According to our observations, junctional tightness as well as morphological appearance under the influence of HC is mediated by the cytoskeleton. Cell elasticity measurements on living cells represent intracellular events and morphological changes without any interference of fixation procedures, which normally contain permeabilization and desiccation steps, thus destroying the natural environment of the cells.

SFM, as a surface sensitive technique, is shown to be an adequate tool for investigating intracellular events.

Tilman E. Schäffer thanks the Gemeinnützige Hertie Stiftung/Stifterverband für die Deutsche Wissenschaft for financial support.

REFERENCES

1. Reese, T. S., and M. J. Karnovsky. 1967. Structural localization of a blood-brain barrier to exogenous peroxidase. *J. Cell Biol.* 34:207–217.
2. Brightman, M. W., and T. S. Reese. 1969. Junctions between intimately apposed cell membranes in the vertebrate brain. *J. Cell Biol.* 40:648–677.
3. Brightman, M. W., I. Klatzo, Y. Olsson, and T. S. Reese. 1970. The blood-brain barrier to proteins under normal and pathological conditions. *J. Neurol. Sci.* 10:215–239.
4. Oldendorf, W. H., S. Hyman, L. Braun, and S. Z. Oldendorf. 1972. Blood-brain barrier: penetration of morphine, codeine, heroin, and methadone after carotid injection. *Science.* 178:984–986.
5. Pratt, J., J. Rataud, F. Bardot, M. Roux, J. C. Blanchard, P. M. Laduron, and J. M. Stutzmann. 1992. Neuroprotective actions of riluzole in rodent models of global and focal cerebral ischaemia. *Neurosci. Lett.* 140:225–230.
6. Eisenblaetter, T., S. Huewel, and H. J. Galla. 2003. Characterisation of the brain multidrug resistance protein (BMDP/ABCG2/BCRP) expressed at the blood-brain barrier. *Brain Res.* 971:221–231.
7. Hoheisel, D., T. Nitz, H. Franke, J. Wegener, A. Hakvoort, T. Tilling, and H. J. Galla. 1998. Hydrocortisone reinforces the blood-brain barrier properties in a serum free cell culture system. *Biochem. Biophys. Res. Commun.* 244:312–316.
8. Wolburg, H., J. Neuhaus, U. Kniesel, B. Krauss, E. M. Schmid, M. Ocalan, C. Farrell, and W. Risau. 1994. Modulation of tight junction structure in blood-brain barrier endothelial cells. Effects of tissue culture, second messengers and cocultured astrocytes. *J. Cell Sci.* 107:1347–1357.
9. Nagy, Z., H. Peters, and I. Huttner. 1984. Fracture faces of cell junctions in cerebral endothelium during normal and hyperosmotic conditions. *Lab. Invest.* 50:313–322.
10. Nitz, T., T. Eisenblaetter, K. Psathaki, and H. J. Galla. 2003. Serum-derived factors weaken the barrier properties of cultured porcine brain capillary endothelial cells in vitro. *Brain Res.* 981:30–40.
11. Henderson, E., P. G. Haydon, and D. S. Sakaguchi. 1992. Actin filament dynamics in living glial cells imaged by atomic force microscopy. *Science.* 257:1944–1946.
12. Tao, N. J., and S. Lindsay. 1992. M, Lees, S. Measuring the microelastic properties of biological material. *Biophys. J.* 63:1165–1169.
13. Hoh, J. H., and P. K. Hansma. 1992. Atomic force microscopy for high-resolution imaging in cell biology. *Trends Cell Biol.* 2:208–213.
14. Radmacher, M., J. P. Cleveland, M. Fritz, H. G. Hansma, and P. K. Hansma. 1994. Mapping interaction forces with the atomic force microscope. *Biophys. J.* 66:2159–2165.
15. Radmacher, M., M. Fritz, and P. K. Hansma. 1995. Imaging soft samples with the atomic force microscope: gelatin in water and propanol. *Biophys. J.* 69:264–270.
16. Jiao, Y., and T. E. Schäffer. 2004. Accurate height and volume measurements on soft samples with the atomic force microscope. *Langmuir.* 20:10038–10045.
17. Hertz, H. 1882. Über die Berührung fester elastischer Körper *J. Reine Angewandte Mathematik.* 92:156–171. [in German].
18. Sneddon, I. N. 1965. The relation between load and penetration in the axissymmetric Boussinesq problem for a punch of arbitrary profile. *Int. J. Eng. Sci.* 3:47–57.
19. Jiao, Y., D. I. Cherny, G. Heim, T. M. Jovin, and T. E. Schaffer. 2001. Dynamic interactions of p53 with DNA in solution by time-lapse atomic force microscopy. *J. Mol. Biol.* 314:233–243.
20. Franke, H., H. J. Galla, and C. T. Beuckmann. 2000. Primary cultures of brain microvessel endothelial cells: a valid and flexible model to study drug transport through the blood-brain barrier in vitro. *Brain Res. Brain Res. Protoc.* 5:248–256.
21. Deli, M. A., C. S. Abraham, M. Niwa, and A. N. Falus. 2003. N-diethyl-2-[4-(phenylmethyl)phenoxy]ethanamine increases the permeability of primary mouse cerebral endothelial cell monolayers. *Inflamm. Res.* 52(Suppl. 1):39–40.
22. Butt, H.-J., and M. Jaschke. 1995. Calculation of thermal noise in atomic force microscopy. *Nanotechnology.* 6:1–7.
23. Fanning, A. S., L. L. Mitic, and J. M. Anderson. 1999. Transmembrane proteins in the tight junction barrier. *J. Am. Soc. Nephrol.* 10:1337–1345.
24. Tsukita, S., A. Nagafuchi, and S. Yonemura. 1992. Molecular linkage between cadherins and actin filaments in cell-cell adherens junctions. *Curr. Opin. Cell Biol.* 4:834–839.
25. Katsube, T., M. Takahisa, R. Ueda, N. Hashimoto, M. Kobayashi, and S. Togashi. 1998. Cortactin associates with the cell-cell junction protein ZO-1 in both Drosophila and mouse. *J. Biol. Chem.* 273: 29672–29677.
26. Mattagajasingh, S. N., S. C. Huang, J. S. Hartenstein, and E. J. Benz, Jr. 2000. Characterization of the interaction between protein 4.1R and ZO-2. A possible link between the tight junction and the actin cytoskeleton. *J. Biol. Chem.* 275:30573–30585.
27. Radmacher, M. 2002. Measuring the elastic properties of living cells by the atomic force microscope. *Methods Cell Biol.* 68:67–87.
28. Sackmann, E. 1994. Intra- and extracellular macromolecular networks: physics and biological function. *Macromol. Chem. Phys.* 195:7–28.
29. Ringold, G. M. 1985. Steroid hormone regulation of gene expression. *Annu. Rev. Pharmacol. Toxicol.* 25:529–566.
30. Castellino, F., J. Heuser, S. Marchetti, B. Bruno, and A. Luini. 1992. Glucocorticoid stabilization of actin filaments: a possible mechanism for inhibition of corticotropin release. *Proc. Natl. Acad. Sci. USA.* 89:3775–3779.
31. Inoué, S. 1981. Cell division and the mitotic spindle. *J. Cell Biol.* 91:131–147.
32. Salmon, E. D., M. McKeel, and T. Hays. 1984. Rapid rate of tubulin dissociation from microtubules in the mitotic spindle in vivo measured by blocking polymerization with colchicine. *J. Cell Biol.* 99:1066–1075.
33. Manfredi, J. J., J. Parness, and S. B. Horwitz. 1982. Taxol binds to cellular microtubules. *J. Cell Biol.* 94:688–696.
34. Rotsch, C., and M. Radmacher. 2000. Drug-induced changes of cytoskeletal structure and mechanics in fibroblasts: an atomic force microscopy study. *Biophys. J.* 78:520–535.
35. Bergmann, J. E., A. Kupfer, and S. J. Singer. 1983. Membrane insertion at the leading edge of motile fibroblasts. *Proc. Natl. Acad. Sci. USA.* 80:1367–1371.
36. Alberts, B., A. Johnson, J. Lewis, M. Raff, K. Roberts, and P. Walter. 2002. Molecular Biology of the Cell. Taylor & Francis Books, London, UK.
37. Haga, H., S. Sasaki, K. Kawabata, E. Ito, T. Ushiki, and T. Sambongi. 2000. Elasticity mapping of living fibroblasts by AFM and immunofluorescence observation of the cytoskeleton. *Ultramicroscopy.* 82: 253–258.
38. Goerge, T., A. Niemeyer, P. Rogge, R. Ossig, H. Oberleithner, and S. W. Schneider. 2002. Secretion pores in human endothelial cells during acute hypoxia. *J. Membr. Biol.* 187:203–211.
39. Weidenfeller, Ch., A. Zozulya, S. Schrot, and H.-J.Galla. 2005. Murine brain capillary endothelial cells exhibit improved barrier properties under the influence of hydrocortisone. *Brain Res.* 1053:162–174.